magnetochemistry

MDPI

Article

How to Quench Ferromagnetic Ordering in a CN-Bridged Ni(II)-Nb(IV) Molecular Magnet? A Combined High-Pressure Single-Crystal X-Ray Diffraction and Magnetic Study

Gabriela Handzlik [1], Barbara Sieklucka [1], Hanna Tomkowiak [2], Andrzej Katrusiak [2] and Dawid Pinkowicz [1,*]

1 Faculty of Chemistry, Jagiellonian University, Gronostajowa 2, 30-387 Kraków, Poland; gabriela.handzlik@uj.edu.pl (G.H.); barbara.sieklucka@uj.edu.pl (B.S.)
2 Faculty of Chemistry, Adam Mickiewicz University, Umultowska 89b, 61-614, Poznań, Poland; hannat@amu.edu.pl (H.T.); katran@amu.edu.pl (A.K.)
* Correspondence: dawid.pinkowicz@uj.edu.pl; Tel.: +48-12-686-2457

Received: 12 April 2019; Accepted: 28 May 2019; Published: 1 June 2019

Abstract: High-pressure (HP) structural and magnetic properties of a magnetic coordination polymer $\{[Ni^{II}(pyrazole)_4]_2[Nb^{IV}(CN)_8]\cdot 4H_2O\}_n$ (Ni_2Nb) are presented, discussed and compared with its two previously reported analogs $\{[Mn^{II}(pyrazole)_4]_2[Nb^{IV}(CN)_8]\cdot 4H_2O\}_n$ (Mn_2Nb) and $\{[Fe^{II}(pyrazole)_4]_2[Nb^{IV}(CN)_8]\cdot 4H_2O\}_n$ (Fe_2Nb). Ni_2Nb shows a significant decrease of the long-range ferromagnetic ordering under high pressure when compared to Mn_2Nb, where the pressure enhances the T_c (magnetic ordering temperature), or to Fe_2Nb exhibiting a pressure-induced spin crossover. The different HP magnetic responses of the three compounds were rationalized and correlated with the structural models as determined by single-crystal X-ray diffraction.

Keywords: ferromagnetism; long-range magnetic ordering; X-ray diffraction; high pressure; nickel(II); octacyanidoniobate(IV); coordination polymers

1. Introduction

Structural and magnetic measurements under high pressure are the most reliable source of straightforward magneto-structural correlations in crystalline magnetic solids. These types of studies make it possible to fine-tune the structure and physical properties in a continuous manner—a feature that cannot be achieved via chemical modifications, which often introduce unexpected complications (different packing modes, additional intra- and intermolecular contacts). The application of high pressure is known to be extremely useful for enhancing the magnetic ordering temperature of extended coordination systems [1–5], ligand field and magnetic anisotropy tuning of mononuclear complexes [6,7] and control of the spin crossover behavior [8,9]. The combined high-pressure single-crystal X-ray diffraction (scXRD) and SQUID magnetometry make a perfect set of tools to study and understand the changes induced by this type of mechanical stimulus. scXRD structural analysis experiments are commonly performed using diamond anvil cells (DACs) [10] and, in the case of high-pressure SQUID magnetometry, the most common environment chamber is a piston-cylinder cell (PCC) made of diamagnetic copper-beryllium alloy [11].

Magnetic coordination polymers are known for their high responsiveness to mechanical stress and high pressure. In particular, cyanide-bridged Prussian Blue analogs [12] and the related octacyanometallate-based bimetallic assemblies [2] show significant magnetic changes under high pressure.

Herein, we present the quenching of the long-range ferromagnetic ordering in a cyanide-bridged coordination polymer $\{[Ni^{II}(pyrazole)_4]_2[Nb^{IV}(CN)_8]\cdot 4H_2O\}_n$ (Ni_2Nb) based on nickel(II) (S = 1) and niobium(IV) ($S = \frac{1}{2}$). We also discuss its properties in comparison to Mn^{II} and Fe^{II} analogs: $\{[Mn^{II}(pyrazole)_4]_2[Nb^{IV}(CN)_8]\cdot 4H_2O\}_n$ (Mn_2Nb) and $\{[Fe^{II}(pyrazole)_4]_2[Nb^{IV}(CN)_8]\cdot 4H_2O\}_n$ (Fe_2Nb) [13].

2. Results and Discussion

2.1. X-ray Crystal Structure Description under High Pressure

Ni_2Nb shows some interesting structural distortions when pressurized using a Merrill–Bassett DAC [14]. Its structure under pressure was determined by scXRD (Figure 1 and Table 1) [13]. Ni_2Nb crystallizes in a tetragonal space group $I4_1/a$ and forms a three-dimensional (3-D) CN-bridged skeleton with a flattened diamond-like topology where the niobium and nickel ions are all linked by cyanide ligands. The niobium(IV) centers play the role of the four-fold tetrahedral nodes in the 3-D framework of Ni_2Nb (Figure 1a,b).

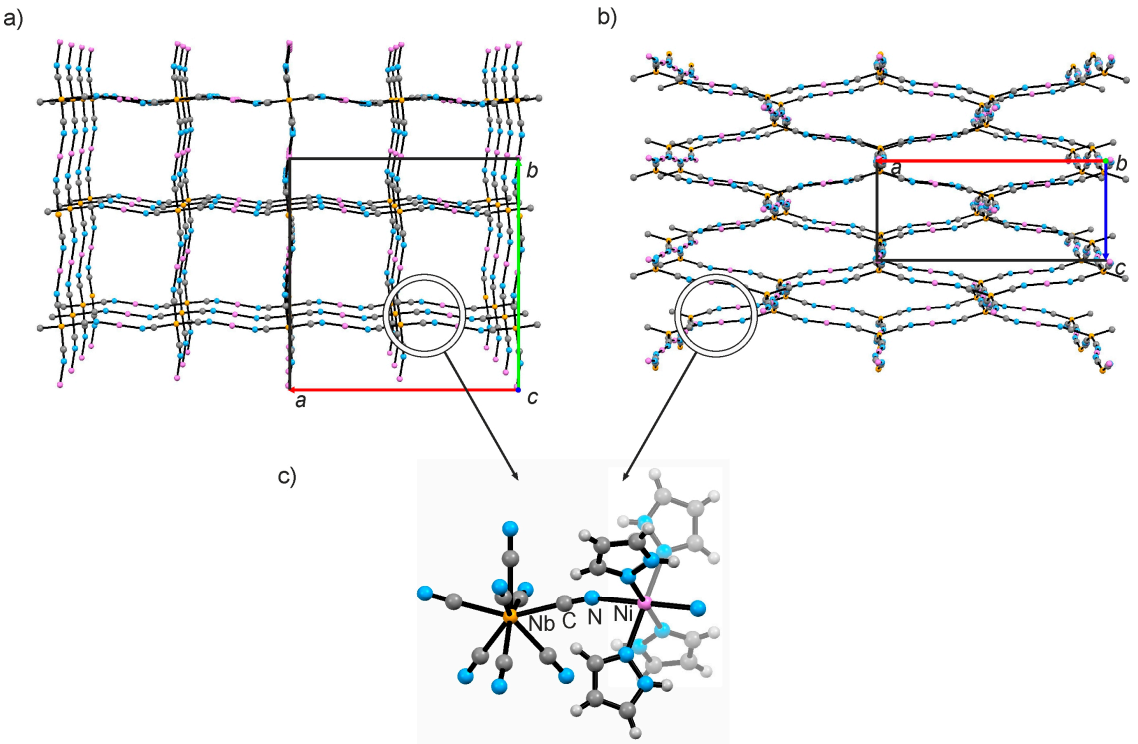

Figure 1. Structural diagrams presenting the cyanido-bridged framework of $\{[Ni^{II}(pyrazole)_4]_2[Nb^{IV}(CN)_8]\cdot 4H_2O\}_n$ down crystallographic axis z (**a**) and axis x (**b**). H_2O, pyrazole and non-bridging CN^- are omitted for clarity. (**c**) The local geometry of the Nb^{IV}-CN-Ni^{II} structural motif.

Table 1. Single-crystal X-ray diffraction (scXRD) unit-cell parameters for Ni_2Nb at room temperature and high pressure.

Formula	$C_{32}H_{40}N_{24}NbNi_2O_4$
Temperature, K	296(2)
λ, Å	0.71073 Å
Molecular weight, g/mol	1035.11
Crystallographic system	tetragonal
Space group	$I4_1/a$
0.0001 GPa	
Unit cell, Å	a = 21.4340(4)
	c = 9.6410(2)
Volume V, Å^3	V = 4429.23(15)
0.25(2) GPa	
Unit cell, Å	a = 21.2935(17)
	c = 9.584(2)
Volume V, Å^3	V = 4345.0(10)
0.61(2) GPa	
Unit cell, Å	a = 21.2002(7)
	c = 9.4404(5)
Volume V, Å^3	V = 4243.0(3)
1.00(2) GPa	
Unit cell, Å	a = 21.0921(13)
	c = 9.3306(11)
Volume V, Å^3	V = 4151.0(6)
1.30(2) GPa	
Unit cell, Å	a = 20.9721(8)
	c = 9.292(2)
Volume V, Å^3	V = 4087.1(1)
1.50(2) GPa	
Unit cell, Å	a = 20.8535(18)
	c = 9.219(7)
Volume V, Å^3	V = 4009(3)
1.88(2) GPa	
Unit cell, Å	a = 20.8438(9)
	c = 9.184(4)
Volume V, Å^3	V = 3990.3(17)
2.15(2) GPa	
Unit cell, Å	a = 20.704(10)
	c = 9.167(7)
Volume V, Å^3	V = 3930(4)
2.48(2) GPa	
Unit cell, Å	a = 20.635(16)
	c = 9.121(6)
Volume V, Å^3	V = 3884(5)

The high-pressure compression of Ni_2Nb is presented in Table 1 and Figure 2 as the pressure dependence of the normalized unit-cell volume V/V_0, where V_0 is the unit-cell volume at 1000 hPa, along with the relevant data for the two analogs Mn_2Nb and Fe_2Nb published previously [8]. The unit-cell volumes of Mn_2Nb, Fe_2Nb and Ni_2Nb are significantly compressed up to 87.6%, 84.6% and

87.7% of the initial value at ca. 2.4 GPa, respectively. The V/V_0 vs. p dependences were fitted using the third-order Birch-Murnaghan equation of state (BMEOS) [15,16] (Equation (1)):

$$p(V) = \frac{3K_0}{2}\left[\left(\frac{V_0}{V}\right)^{\frac{7}{3}} - \left(\frac{V_0}{V}\right)^{\frac{5}{3}}\right]\left\{1 + \frac{3}{4}\left(K'_0 - 4\right)\left[\left(\frac{V_0}{V}\right)^{\frac{2}{3}} - 1\right]\right\} \quad (1)$$

where p—pressure, V_0—volume at zero pressure, in this case the ambient pressure, V—volume, K_0—isothermal bulk modulus at zero pressure, K'_0—dimensionless first derivative of K_0 with respect to pressure. The solid lines in Figure 2, which represent the best fit to Equation (1), match the experimental data for Ni_2Nb and Mn_2Nb in the investigated pressure range. In the case of Fe_2Nb there is a strong deviation from the BMEOS above 1 GPa. The best fit parameters K_0 and K_0' are: 10.7 ± 0.9 and 8.7 ± 1.8 GPa for Mn_2Nb, 10.4 ± 1.6 and 8.2 ± 5.6 GPa for Fe_2Nb (from the 0–1 GPa range fit) and 11.9 ± 1.2 and 6.9 ± 2.0 GPa in the case of Ni_2Nb. The bulk modulus K_0 value is identical for all isomorphs within the experimental error and quite similar to other molecule-based coordination compounds [6,17,18]. Noteworthy, the K_0 for the studied coordination polymers are nearly two orders of magnitude smaller than for diamond (440 GPa) and only one order larger than for rubber (1 GPa) [19]. This places the mechanical properties of coordination polymers somewhere between typical inorganic solids and soft matter.

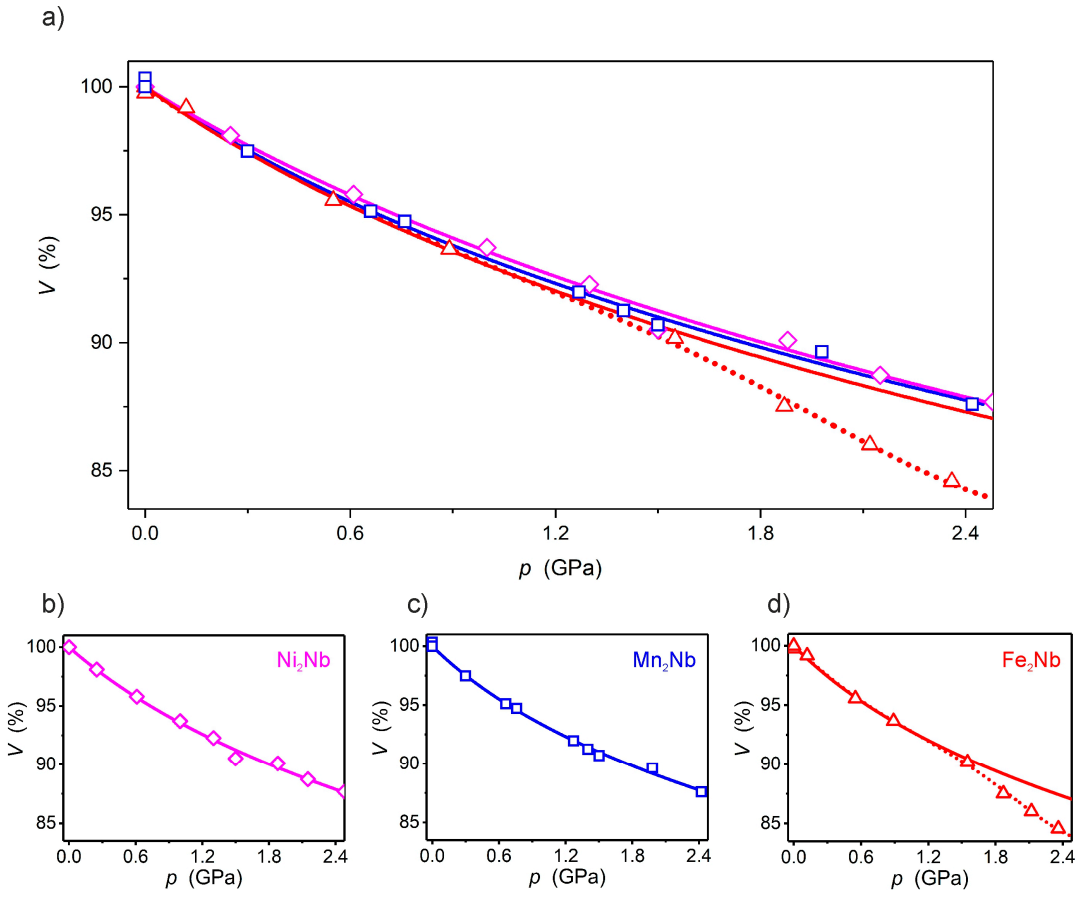

Figure 2. Combined graph (**a**) of $V/V_0(p)$ dependencies for Ni_2Nb (magenta) (**b**), Mn_2Nb (blue) (**c**) and Fe_2Nb (red) (**d**). The solid lines are the best fit to the Birch–Murnaghan equation of state (BMEOS). The dotted line for Fe_2Nb above 1.2 GPa is only a guide for the eye.

The analysis of the coordination spheres of Ni^{II} and Nb^{IV} in Ni_2Nb under high pressure leads to similar observations as for Mn_2Nb [8]: the Nb–C and C–N distances as well as Nb–C–N angles remain roughly unchanged, while the Ni–N bonds (Figure 3a) shrink significantly in a linear fashion

(Figure 3b). This fact and the good match between the $V/V_0(p)$ dependence and the BMEOS both indicate that no pressure-induced phase transition occurs at room temperature in Ni_2Nb and Mn_2Nb. In fact, the behavior of these two solids is very similar while that of Fe_2Nb is quite different and strongly deviates from BMEOS due to the SCO (SCO - spin crossover) behavior. Also, the Fe–N distances shrink in a non-linear fashion in Fe_2Nb above 1.5 GPa.

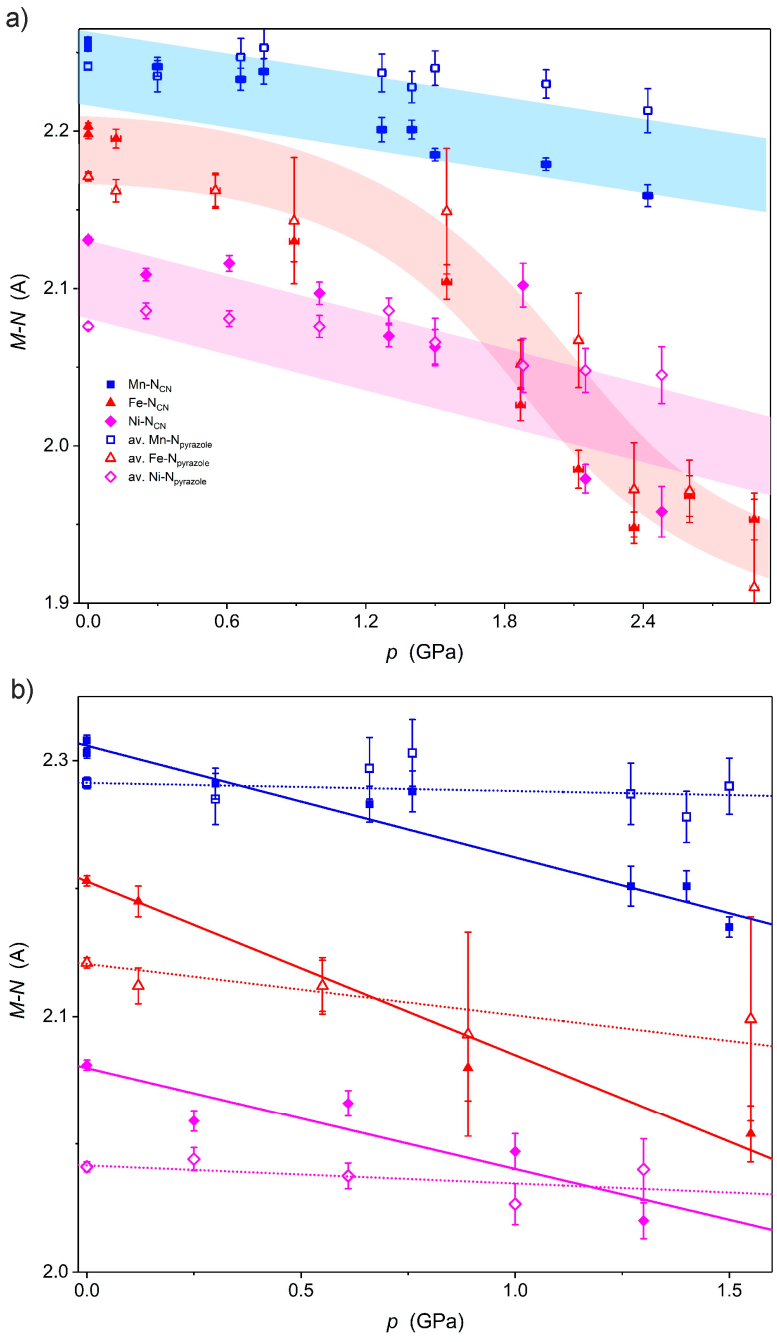

Figure 3. Pressure dependence of the M–N_{CN} bond lengths (full symbols) and M–$N_{pyrazole}$ (open symbols) in the full pressure range (**a**) and in the pressure range where only linear changes are observed (**b**) for Ni_2Nb (magenta), Mn_2Nb (blue) and Fe_2Nb (red). Highlights in (a) are only for guiding the eye, while the lines in (b) are the best linear fit: solid for M–N_{CN} and dotted for M–$N_{pyrazole}$.

A more detailed analysis of M–N bonds up to 1.5 GPa (Ni_2Nb, Mn_2Nb and Fe_2Nb follow the BMEOS in this pressure range) demonstrates that M–N_{CN} shrinkage is much larger than that of M–$N_{pyrazole}$ (Figure 3b and Table 2). As a result, the elongated octahedral coordination spheres of Fe^{II} in Fe_2Nb and Ni^{II} in Ni_2Nb become closer to a perfect octahedron at around 0.7 and 1.2 GPa, respectively.

Table 2. Shrinkage of the M–N_{CN} and M–$N_{pyrazole}$ bonds under pressure. The Δ(M–N)/Δp values are the slopes of the best linear fit from Figure 3b.

	Mn_2Nb	Fe_2Nb	Ni_2Nb
Δ(M-N_{CN})/Δp (Å GPa^{-1})	−0.044	−0.067	−0.040
Δ(M-$N_{pyrazole}$)/Δp (Å GPa^{-1})	−0.003	−0.020	−0.007

2.2. Magnetic Properties under High Pressure

The magnetic properties of Mn_2Nb and Fe_2Nb (Figures 4 and 5, respectively) have been discussed in detail in a previous report [8]. It was established that at ambient pressure both Mn_2Nb and Fe_2Nb are ferrimagnets with long-range magnetic ordering temperatures (T_c) of 23.4 and 9.4 K, respectively. However, the behavior of these compounds under high pressure is very different. Mn_2Nb (Figure 4) displays a very strong and linear increase of the T_c from 23.4 K at ambient pressure to 36.5 K at 1.03 GPa. The linear fit of the $T_c(p)$ dependence (Figure 4c) leads to dT_c/dp = 12.4 ± 0.2 K GPa^{-1}, typical for octacyanidoniobate(IV)-based systems and Prussian Blue analogs [2]. Fe_2Nb, on the other hand, exhibits almost complete quenching of the long-range magnetic ordering under pressure, resulting in paramagnetic properties above 0.7 GPa (Figure 5).

Ni_2Nb is a ferromagnet due to the local ferromagnetic interactions between Nb^{IV} and Ni^{II} ions [13] with the Curie temperature (T_C) of 13.2 K. It exhibits a completely different type of magnetic response to high pressure (Figure 6) when compared to the other two analogs Mn_2Nb and Fe_2Nb. The T_C of Ni_2Nb decreases with increasing pressure, which is characteristic for ferromagnets [20,21], and confirms the presence of local ferromagnetic interactions between Nb^{IV} and Ni^{II}. The T_C shift is 1.9 K GPa^{-1}, as obtained from the linear fit of the $T_C(p)$ dependence (Figure 6c, T_C is the position of the $d\chi/dT$ peak in the $\chi(T)$ measurement at 10 Oe). The pressure response of Ni_2Nb is much weaker and opposite to Mn_2Nb, where the antiferromagnetic interactions between Nb^{IV} and Mn^{II} are present. Hence, the underlying local magnetic interactions in Ni_2Nb (ferromagnetic) vs. Mn_2Nb (antiferromagnetic) are the source of the observed difference. The shortening of the Ni–N_{CN} bonds favors the resonance integral and makes the antiferromagnetic contribution to the total exchange interaction stronger while destabilizing the ferromagnetic one. Overall, the J_{NiNb} coupling constant decreases under pressure.

Ni_2Nb does not present a loss of the magnetic moment under high pressure, which is confirmed by the pressure-independent magnetization at saturation values of 5.3 Nβ (at 2.0 K and 7 T; Figure 6b) up to 1.10 GPa and the structural pressure response that matches the BMEOS. The magnetization at saturation values are close to 5.2 Nβ, as expected for two Ni^{II} (S = 1) and one Nb^{IV} ($S = \frac{1}{2}$) coupled ferromagnetically (assuming g_{Nb} = 2.0 and g_{Ni} = 2.1 [22]).

Ni_2Nb also shows interesting pressure-induced changes in the $M(H)$ dependencies in the 0.1–5 T magnetic field range (Figure 6b). Following the initial sharp increase of the magnetization around 0.05 T in each case, there is a clear dependence with $M(H)$ attaining lower values at higher pressure. All $M(H)$ curves "meet" again above 5 T, converging to the same saturation value of 5.3 Nβ. This behavior is most probably related to the changes of the magnetic anisotropy of the Ni^{II} centers arising from the shortening of the Ni–N_{CN} bonds along the CN–Ni–CN axis of the Ni^{II} coordination sphere, as evidenced by high-pressure structural studies (Figure 3b). The contribution of $[Nb^{IV}(CN)_8]^{4-}$ to the pressure-induced magnetic anisotropy change in the M_2Nb family can be excluded based on the fact that $M(H)$ for Mn_2Nb does not change at all with increasing pressure (Figure 4b).

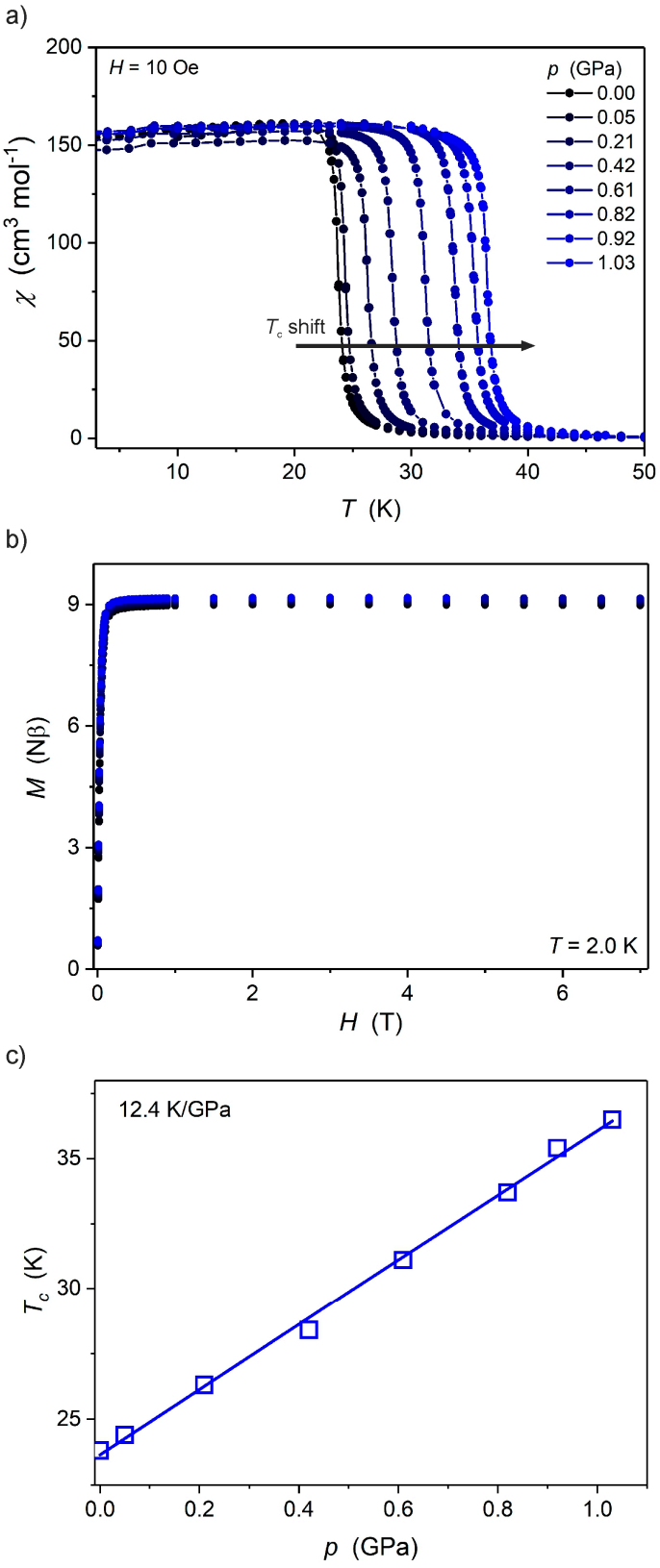

Figure 4. Temperature dependence of molar magnetic susceptibility $\chi(T)$ at 10 Oe (**a**), $M(H)$ at 2.0 K (**b**) and $T_c(p)$ (**c**) for Mn_2Nb under high pressure. The solid line in (a) is only a guide for the eye, while in (c) it represents the best linear fit.

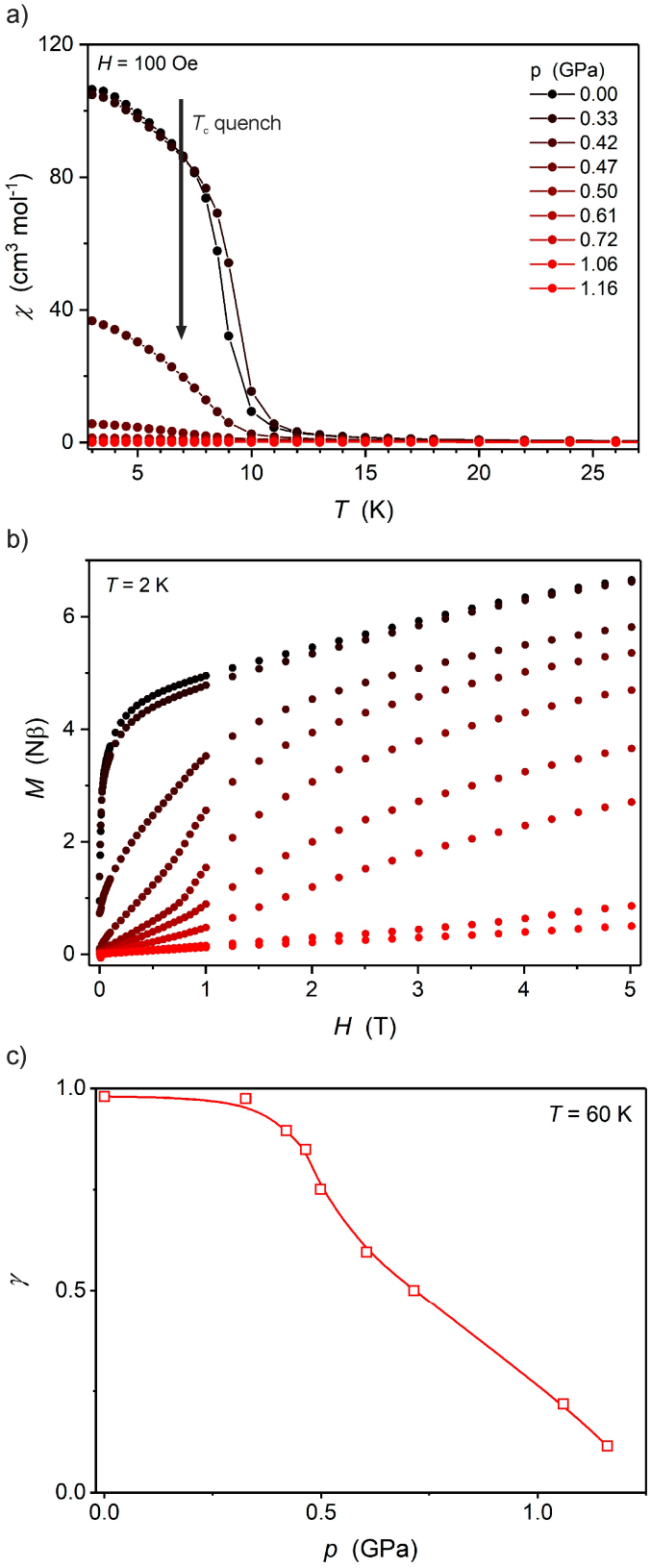

Figure 5. Temperature dependence of molar magnetic susceptibility $\chi(T)$ at 100 Oe (**a**), $M(H)$ at 2.0 K (**b**) and fraction of the high-spin Fe^{II} $\gamma(p)$ at 60 K (**c**) for Fe_2Nb under high pressure. The solid lines in (**a**,**c**) are only guides for the eye.

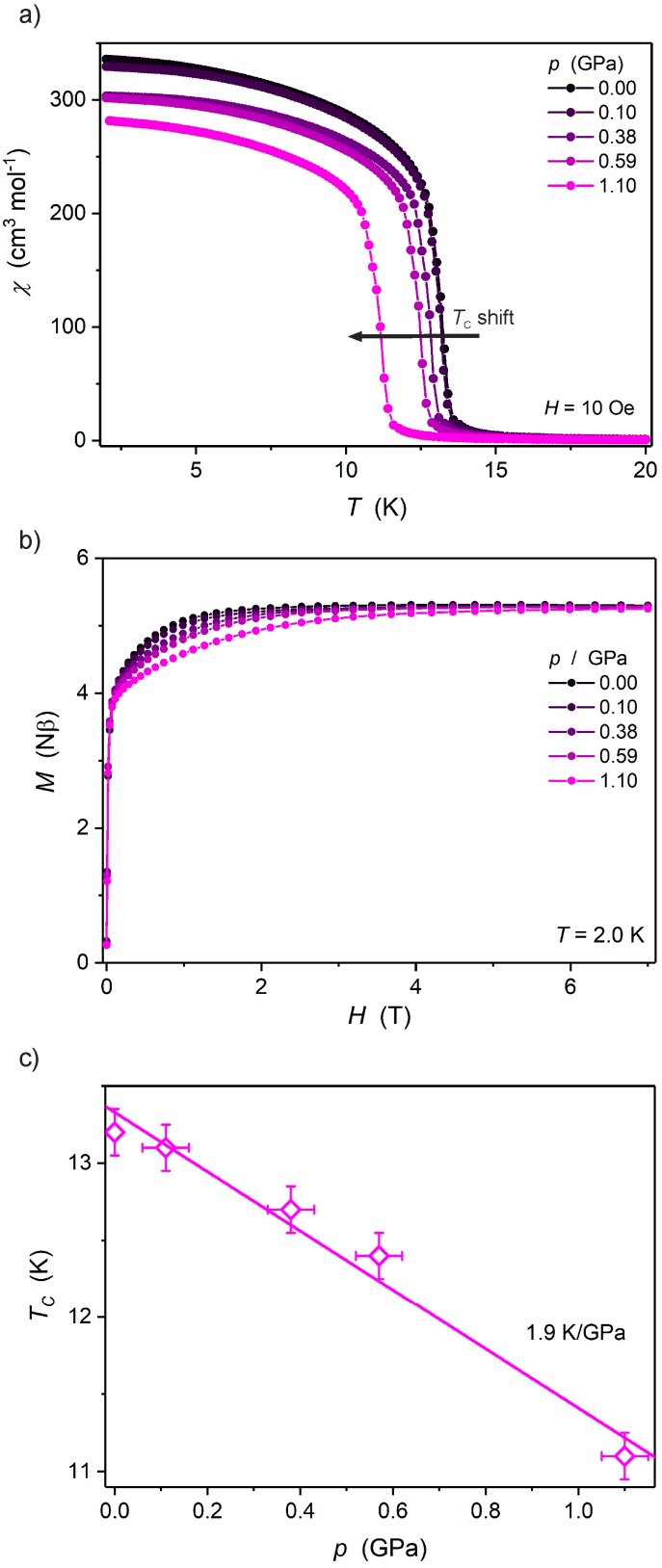

Figure 6. Temperature dependence of molar magnetic susceptibility $\chi(T)$ at 10 Oe (**a**), $M(H)$ at 2.0 K (**b**) and $T_c(p)$ (**c**) for Ni_2Nb under high pressure. The solid lines in (**a**,**b**) are only guides for the eye, while in (**c**) it represents the best linear fit.

3. Materials and Methods

3.1. Materials

Chemicals used in this study were of analytical grade and were obtained from commercial sources (Sigma-Aldrich Co., Avantor, Alfa-Aesar). $K_4[Nb(CN)_8]\cdot 2H_2O$ was prepared according to the newest available procedure [23]. $\{[Ni^{II}(pyrazole)_4]_2[Nb^{IV}(CN)_8]\cdot 4H_2O\}_n$ (Ni_2Nb) was obtained according to the literature procedure and its purity/identity was confirmed by elemental analysis and powder X-ray diffraction, which were identical to those published previously [13].

3.2. Single-Crystal X-ray Diffraction under Pressure

The single crystal diffraction data for Ni_2Nb were collected at room temperature for a single crystal placed in a Merrill–Bassett DAC filled with Fluorinert 77 as the pressure transmitting medium and a chip of ruby. The ruby fluorescence method was used for the pressure determination inside the DAC chamber. The diffraction frames were collected on KUMA KM4-CCD and Xcalibur EOS machines (running Crysalis software; instruments presently manufactured by Rigaku Oxford Diffraction) using a Mo Kα radiation source and a graphite monochromator (λ = 0.71073 Å). The data were corrected for the sample and DAC absorption as well as the for the gasket shadow [24]. Overlaps with the diamond reflections were excluded from the refinement. Non-H atoms were refined anisotropically (weighted full-matrix least-squares on F^2) [25]. The summary of crystallographic data can be found in Table 1. The Cambridge Crystallographic Data Center (CCDC) 1909715–1909722 contains the detailed supplementary crystallographic information for this paper. The crystallographic information files (CIFs) can be obtained free of charge from the CCDC via ww.ccdc.cam.ac.uk/data_request/cif.

The details of the related single-crystal XRD measurements under pressure for Mn_2Nb and Fe_2Nb were reported previously [8].

3.3. Magnetic Measurements under Pressure

Magnetic measurements under pressure for Mn_2Nb and Fe_2Nb were reported previously [8]. Ni_2Nb was characterized in a similar fashion using a Quantum Design MPMS3 SQUID-VSM (Sand Diego, USA) magnetometer. A powdered sample of Ni_2Nb was loaded into the CuBe piston-cylinder cell (manufactured by HMD, Japan; purchased from Quantum Design) with a piece of high-purity lead as the manometer and Daphne 7373 oil as the pressure-transmitting medium. The pressure determination at low temperature was performed with 0.02 GPa accuracy by using the linear pressure dependence of the superconducting transition of Pb (−0.379 K GPa^{-1}). Magnetic data were corrected for the diamagnetic contribution of the sample and the pressure cell.

4. Conclusions

A combined high-pressure magneto-structural study of a magnetic coordination polymer $\{[Ni^{II}(pyrazole)_4]_2[Nb^{IV}(CN)_8]\cdot 4H_2O\}_n$ Ni_2Nb was carried out and revealed a strong magnetic response of this material to mechanical stress. The magnetic ordering temperature of Ni_2Nb shifted linearly towards lower temperatures at higher pressure due to the ferromagnetic character of the exchange coupling between Nb^{IV} and Ni^{II} ions. Such behavior is completely different from that observed for the two analogs $\{[Mn^{II}(pyrazole)_4]_2[Nb^{IV}(CN)_8]\cdot 4H_2O\}_n$ Mn_2Nb and $\{[Fe^{II}(pyrazole)_4]_2[Nb^{IV}(CN)_8]\cdot 4H_2O\}_n$ Fe_2Nb. Mn_2Nb exhibited an opposite effect—a strong enhancement of T_c under pressure due to the antiferromagnetic exchange coupling between the constituent magnetic ions. Our study confirms the usefulness of combined high-pressure studies to understand the magnetic properties of molecular magnets and the possibility to fine-tune their properties by applying a mechanical stimulus—namely, high pressure.

Author Contributions: D.P. conceived and designed the experiments, performed the magnetic measurements and wrote the first draft of the paper; G.H. participated in the high-pressure magnetic measurements; H.T. and A.K. performed the high pressure scXRD measurements and analyzed the data; all authors participated in the preparation of the final version of the manuscript.

Funding: This research was funded by the Polish National Science Centre within the Sonata Bis project (2016/22/E/ST5/00055).

Conflicts of Interest: The authors declare no conflict of interest.

References

1. Woodall, C.H.; Craig, G.A.; Prescimone, A.; Misek, M.; Cano, J.; Faus, J.; Probert, M.R.; Parsons, S.; Moggach, S.; Martínez-Lillo, J.; et al. Pressure induced enhancement of the magnetic ordering temperature in rhenium(IV) monomers. *Nat. Commun.* **2016**, *7*, 13870. [CrossRef] [PubMed]
2. Pinkowicz, D.; Kurpiewska, K.; Lewiński, K.; Bałanda, M.; Mihalik, M.; Sieklucka, M.Z.B. High-pressure single-crystal XRD and magnetic study of a octacyanoniobate-based magnetic sponge. *CrystEngComm* **2012**, *14*, 5224–5229. [CrossRef]
3. Coronado, E.; Giménez-López, M.C.; Korzeniak, T.; Levchenko, G.; Romero, F.M.; Segura, A.; Garcia-Baonza, V.; Cezar, J.C.; de Groot, F.M.; Milner, A.; et al. Pressure-Induced Magnetic Switching and Linkage Isomerism in K0.4Fe4[Cr(CN)6]2.8·16H2O: X-ray Absorption and Magnetic Circular Dichroism Studies. *J. Am. Chem. Soc.* **2008**, *130*, 15519–15532. [CrossRef] [PubMed]
4. Ohba, M.; Kaneko, W.; Kitagawa, S.; Maeda, T.; Mito, M. Pressure Response of Three-Dimensional Cyanide-Bridged Bimetallic Magnets. *J. Am. Chem. Soc.* **2008**, *130*, 4475–4484. [CrossRef] [PubMed]
5. Shum, W.W.; Her, J.H.; Stephens, P.W.; Lee, Y.; Miller, J.S. Observation of the Pressure Dependent Reversible Enhancement of Tc and Loss of the Anomalous Constricted Hysteresis for [Ru2(O2CMe)4]3[Cr(CN)6]. *Adv. Mater.* **2007**, *19*, 2910–2913. [CrossRef]
6. Craig, G.A.; Sarkar, A.; Woodall, C.H.; Hay, M.A.; Marriott, K.E.; Kamenev, K.V.; Moggach, S.A.; Brechin, E.K.; Parsons, S.; Rajaraman, G.; et al. Rajaraman and M. Murrie. Probing the origin of the giant magnetic anisotropy in trigonal bipyramidal Ni(ii) under high pressure. *Chem. Sci.* **2018**, *9*, 1551–1559. [CrossRef]
7. Prescimone, A.; Sanchez-Benitez, J.; Kamenev, K.K.; Moggach, S.A.; Warren, J.E.; Lennie, A.R.; Murrie, M.; Parsons, S.; Brechin, E.K. High pressure studies of hydroxo-bridged Cu(ii) dimers. *Dalton Trans.* **2010**, *39*, 113–123. [CrossRef]
8. Pinkowicz, D.; Rams, M.; Mišek, M.; Kamenev, K.V.; Tomkowiak, H.; Katrusiak, A.; Sieklucka, B. Enforcing Multifunctionality: A Pressure-Induced Spin-Crossover Photomagnet. *J. Am. Chem. Soc.* **2015**, *137*, 8795–8802. [CrossRef]
9. Gütlich, P.; Ksenofontov, V.; Gaspar, A.B. Pressure effect studies on spin crossover systems. *Coord. Chem. Rev.* **2005**, *249*, 1811–1829. [CrossRef]
10. Katrusiak, A. High-pressure devices. In *International Tables for Crystallography, Volume H, Powder Diffraction*; Gilmore, C.J., Kaduk, J.A., Schenk, H., Eds.; John Wiley & Sons: New York, NY, USA, 2018; pp. 156–173. [CrossRef]
11. Kamarád, J.; Machátová, Z.; Arnold, Z. High pressure cells for magnetic measurements—Destruction and functional tests. *Rev. Sci. Instrum.* **2004**, *75*, 5022–5025. [CrossRef]
12. Awaga, K.; Sekine, T.; Okawa, M.; Fujita, W.; Holmes, S.M.; Girolami, G.S. High-pressure effects on a manganese hexacyanomanganate ferrimagnet with TN = 29K. *Chem. Phys. Lett.* **1998**, *293*, 352–356. [CrossRef]
13. Pinkowicz, D.; Pełka, R.; Drath, O.; Nitek, W.; Bałanda, M.; Majcher, A.M.; Poneti, G.; Sieklucka, B. Nature of Magnetic Interactions in 3D {[MII(pyrazole)$_4$]$_2$[NbIV(CN)$_8$]·4H2O}n (M = Mn, Fe, Co, Ni) Molecular Magnets. *Inorg. Chem.* **2010**, *49*, 7565–7576. [CrossRef]
14. Merrill, L.; Bassett, W.A. Miniature diamond anvil pressure cell for single crystal x-ray diffraction studies. *Rev. Sci. Instrum.* **1974**, *45*, 290–294. [CrossRef]
15. Birch, F. Finite Elastic Strain of Cubic Crystals. *Phys. Rev.* **1947**, *71*, 809–824. [CrossRef]
16. Birch, F. Finite strain isotherm and velocities for single-crystal and polycrystalline NaCl at high pressures and 300 K. *J. Geophys. Res. Solid Earth* **1978**, *83*, 1257–1268. [CrossRef]

17. Byrne, P.J.; Richardson, P.J.; Chang, J.; Kusmartseva, A.F.; Allan, D.R.; Jones, A.C.; Kamenev, K.V.; Tasker, P.A.; Parsons, S. Piezochromism in Nickel Salicylaldoximato Complexes: Tuning Crystal-Field Splitting with High Pressure. *Chem. Eur. J.* **2012**, *18*, 7738–7748. [CrossRef] [PubMed]
18. Madsen, S.R.; Overgaard, J.; Stalke, D.; Iversen, B.B. High-pressure single crystal X-ray diffraction study of the linear metal chain compound $Co_3(dpa)_4Br_2{\cdot}CH_2Cl_2$. *Dalton Trans.* **2015**, *44*, 9038–9043. [CrossRef] [PubMed]
19. Tabor, D. The bulk modulus of rubber. *Polymer* **1994**, *35*, 2759–2763. [CrossRef]
20. Motokawa, N.; Miyasaka, H.; Yamashita, M. Pressure effect on the three-dimensional charge-transfer ferromagnet [{Ru_2(m-FPhCO_2)$_4$}$_2$(BTDA-TCNQ)]. *Dalton Trans.* **2010**, *39*, 4724–4726. [CrossRef] [PubMed]
21. Mito, M.; Matsumoto, K.; Komorida, Y.; Deguchi, H.; Takagi, S.; Tajiri, T.; Iwamoto, T.; Kawae, T.; Tokita, M.; Takeda, K. Volume shrinkage dependence of ferromagnetic moment in lanthanide ferromagnets gadolinium, terbium, dysprosium, and holmium. *J. Phys. Chem. Solids* **2009**, *70*, 1290–1296. [CrossRef]
22. Kataev, V.; Golze, C.; Alfonsov, A.; Klingeler, R.; Büchner, B.; Goiran, M.; Broto, J.M.; Rakoto, H.; Mennerich, C.; Klauss, H.H.; et al. Magnetism of a novel tetranuclear nickel(II) cluster in strong magnetic fields. *J. Phys. Conf. Ser.* **2006**, *51*, 351–354. [CrossRef]
23. Handzlik, G.; Magott, M.; Sieklucka, B.; Pinkowicz, D. Alternative Synthetic Route to Potassium Octacyanidoniobate (IV) and Its Molybdenum Congener. *Eur. J. Inorg. Chem.* **2016**, *2016*, 4872–4877. [CrossRef]
24. Katrusiak, A. Shadowing and absorption corrections of single-crystal high-pressure data. *Zeitschrift Für Kristallographie Crystalline Materials* **2004**, *219*, 461–467. [CrossRef]
25. Sheldrick, G. A short history of SHELX. *Acta Crystallogr. Sect. A Found. Crystallogr.* **2008**, *64*, 112–122. [CrossRef] [PubMed]